Tourette's syndrome that have identified altered relationships between the basal ganglia on the two sides. The nature of this relationship needs to be clarified. Additional studies to evaluate other mechanisms, such as serotonin receptor function, are required to better define the pathophysiology of this disorder.

ACKNOWLEDGMENT

Special thanks to Medi-Physics Inc., Amersham Health Care, Arlington Heights, IL, for supplying the radiopharmaceutical kits used in this study.

REFERENCES

1. Pitman R, Green R, Jenike M, Mesulam M. Clinical comparison of Tourette's disorder and obsessive-compulsive disorder. *Am J Psychiatry* 1987;144:1166–1171.
2. McDowell F, Cedarbaum JM. The extrapyramidal system and disorders of movement. In: Joynt RJ, ed. *Clinical neurology*, Philadelphia: J.B. Lippincott Co.; 1994:71–73.
3. Frankel M, Cummings J, Robertson M, et al. Obsessions and compulsions in Gilles de la Tourette's syndrome. *Neurology* 1986;36:378–382.
4. Chase TN, Geoffrey V, Gillespie M, et al. Structural and functional studies of Gilles de la Tourette's syndrome. *Rev Neurol (Paris)* 1986;142:851–855.
5. Riddle M, Rasmusson A, Woods S, et al. SPECT imaging of cerebral blood flow in Tourette's syndrome. *Adv Neurol* 1992;58:207–211.
6. Sieg K, Buckingham D, Gaffney G, et al. Technetium-99m-HMPAO brain SPECT imaging of Gilles de la Tourette's syndrome. *Clin Nucl Med* 1993;18:255p.
7. Hamlin C, Swayne L, Liebowitz M, et al. Striatal IMP-SPECT decrease in obsessive-compulsive disorder, normalized by pharmacotherapy. *Neuropsych Neuropsychol Behavioral Neurol* 1989;2:290–300.
8. Paterson B, Riddle MA, Cohen DJ, et al. Reduced basal ganglia volumes in Tourette's syndrome using three-dimensional reconstruction techniques from magnetic resonance images. *Neurology* 1993;43:941–949.
9. Singer HS, Reiss AL, Brown JE, et al. Volumetric MRI changes in basal ganglia of children with Tourette's syndrome. *Neurology* 1993;43:950–956.
10. Como PG. Obsessive-compulsive disorder in Tourette's syndrome. *Adv Neurol* 1995; 65: 281–291.
11. Turjanski N, Sawle GV, Playford ED, et al. PET Studies of the presynaptic and postsynaptic dopaminergic system in Tourette's syndrome. *J Neurol Neurosurg Psych* 1994;57:688–692.
12. Singer H, Wong D, Brown J, et al. Positron emission tomography evaluation of dopamine D2 receptors in adults with Tourette's syndrome. *Adv Neurol* 1992;58:233–238.

PET with L-[1-Carbon-11]-Tyrosine to Visualize Tumors and Measure Protein Synthesis Rates

Annemieke C. Kole, Jan Pruim, Omgo E. Nieweg, Robert J. van Ginkel, Harald J. Hoekstra, Heimen Schraffordt Koops and Willem Vaalburg

PET Center and Department of Surgical Oncology, Groningen University Hospital, Groningen; and Department of Surgery, The Netherlands Cancer Institute, Amsterdam, The Netherlands

We studied the potential of PET with L-[1-^{11}C]-tyrosine (TYR) to visualize tumors outside the central nervous system and to quantify their protein synthesis rates (PSRs). **Methods:** Twenty-two patients suspected of having a malignant tumor underwent a PET study with TYR before biopsy. The PSR in nanomoles per milliliter tumor tissue per minute as well as the PSR in contralateral normal tissue, standardized uptake values (SUVs) and tumor-to-nontumor-ratios (T/N ratios) were calculated. **Results:** Fifteen of the 16 malignancies (94%) were correctly visualized as a hot spot. A chondrosarcoma of the sacrum was not visualized. Of the six patients with benign lesions, cold spots were correctly identified in four (67%). A benign schwannoma and an intramuscular hemangioma of the forearm were visualized as hot spots. PSR in tumor tissue was higher than in the corresponding contralateral normal tissues. PSR and SUV in malignant tumors were higher than in benign tumors. **Conclusion:** TYR appears to be a good tracer for imaging malignancies. The PSR, which was higher in malignant tumors than in normal tissue and the studied benign lesions, could be quantified and correlated with the SUV.

Key Words: PET; carbon-11-tyrosine; protein synthesis rate

J Nucl Med 1997; 38:191–195

The potential of PET to diagnose cancer and monitor therapeutic response is widely recognized. Whereas advanced imaging techniques such as CT and MRI are based on the imaging of anatomy, PET enables the visualization of metabolism and (patho)physiology. This complementary information may be advantageous, e.g., detection of metastases (*1–3*). The main disadvantages of PET, i.e., its complexity and high cost, are at this stage outweighed by its higher resolution and greater sensitivity compared to SPECT (*4*). Even with the possibility of performing coincidence measurements with positron emitters in SPECT cameras, the major advantage of PET remains the ability to quantify metabolism, which makes it a powerful tool for grading malignancy and monitoring the effect of therapy (*5*).

So far, 2-[^{18}F]-fluoro-2-deoxy-D-glucose (FDG) has been the most widely used radiopharmaceutical, based on the fact that tumor cells have increased glucose uptake. However, the use of FDG has several disadvantages, such as high background uptake in normal brain tissue, low specificity and uptake in inflammatory tissues (*6,7*). Therefore, there is a need for alternatives. Ishiwata (*8*) has shown that the uptake of amino acids is also high in tumor tissue due to an increased protein synthesis rate (PSR). Amino acids play a minor role in the metabolism of inflammatory cells (mainly neutrophils) compared to FDG (*9,10*). The measurement of ^{11}C-labeled amino acid uptake may be a better way to predict tumor growth rate than the glucose consumption rate measured with FDG. The majority of PET studies seeking to establish its predictive value for grading malignancy (*11,12*) and assess the effect of surgery (*13*) and radiotherapy (*12*) have been performed with L-[methyl-^{11}C]-methionine (MET). MET reflects amino acid uptake rather than protein synthesis. Since MET is involved in other metabolic pathways, such as transmethylation and polyamine synthesis, and it is converted into S-adenosylmethionine, a methyl group donor, which may lead to the accumulation of a variety of nonprotein metabolites in tumor tissue (*14–16*). This complicated metabolism of methionine has made it impossible to create a precise metabolic model. Carboxyl-labeled amino acids, such as L-[1-^{11}C]-tyrosine (TYR) (*17*), L-[1-^{11}C]-methionine (*15*) and L-[1-^{11}C]-leucine (*18*), appear to be more appropriate compounds to determine protein synthesis in tumors, because the main metabolite of these amino acids is $^{11}CO_2$, which is rapidly cleared from tissue and exhaled. Therefore, $^{11}CO_2$ does not contribute substantially to the ^{11}C radioactivity in tumor tissue as measured by PET (*8,19*).

At our institute, a model has been developed to determine the

Received Sept. 14, 1995; revision accepted July 5, 1996.

For correspondence or reprints contact: A.C. Kole, MD, PET Center, University Hospital, PO Box 30001, 9700 RB Groningen, The Netherlands.

PSR in tumor tissue using TYR. The model has been developed (*20*) and validated (*21*) on the basis of animal experiments and data obtained from patients with brain tumors. Initial results in patients with brain tumors have been published recently (*22*). The aims of the present study were to investigate the potential of PET with TYR to visualize various types of tumor outside the central nervous system, to quantify their PSRs and to compare the data with standardized uptake values (SUV).

METHODS

Patients

Twenty-two consecutive patients (9 women, 13 men; aged 21–75 yr; median age 46 yr) referred for oncology outpatient studies participated in the study. The only restriction was that no more than three patients with the same type of tumor be included to prevent the formation of large subgroups. Informed consent was obtained from all the patients. Subjects were suspected of having a malignant tumor based on clinical symptoms and supplementary diagnostics. All PET studies were performed before biopsy and before cancer therapy. To maintain a constant plasma tyrosine level throughout the study, the patients fasted for at least 10 hr (except for water and their usual medication) before the study.

PET Studies

TYR was produced via a modified microwave-induced Bühcher-er-Strecker synthesis (*23*). The radiochemical purity was over 99%. TYR was administered intravenously. Due to variable yields of the synthesis, the injected dose varied from 85 to 374 MBq (median 366).

All PET images were acquired using an ECAT 951/31 PET-camera (Siemens/CTI, Knoxville, TN). This device has a 56-cm diameter patient aperture and acquires 31 planes simultaneously over a 10.8-cm axial field of view. A transmission scan to correct for the photon attenuation by body tissues in the imaged area was obtained immediately before the emission scan. Dynamic scanning with 16 frames was performed from the time of injection to 50 min postinjection at the level of the tumor. These included ten 30-sec images, three 5-min images and three 10-min images. Image data were backprojected using a 0.5 cycle/pixel Hann-filter, which yielded a resolution of 6 mm FWHM.

All PET studies included placement of an arterial canula in the radial artery for sampling arterial blood during data acquisition. First, the nonradiolabeled tyrosine concentration in plasma was measured. In the arterial blood samples, the plasma activity of TYR, the ^{11}C-labeled CO_2 and protein levels were measured by HPLC as described previously (*21*).

PET images were displayed in transaxial projections on a computer display using standard ECAT software. To determine tumor PSR, the tumor must first be defined in all relevant planes of the study. Usually, this is done by placing regions of interest (ROIs) in each plane. The tissue time-activity curves obtained from these ROIs can be averaged and the average PSR can be calculated. As this technique is rather laborious, an alternative method was developed at our institute.

By using the same activity threshold as that used to define the ROI, all voxels in the study above this threshold were selected. The corresponding activity was summed and the average time-activity curve as well as the total volume was obtained. By masking nontumor regions with physiologically high uptake of TYR (e.g., the parotid glands), nontumor regions were prevented from contributing to the average tumor time-activity curve. The advantage of this approach is that the analysis of the whole tumor is performed quickly and simply, while the results are identical to those of the ROI method. By combining this averaged time-activity data with the plasma input data (corrected for $^{11}CO_2$ and ^{11}C-proteins), the average PSR in nanomoles per milliliter tumor tissue per minute was calculated using the modified Patlak analysis as described previously (*21*). The PSR in contralateral normal tissue was calculated using a ROI technique. If the tumor was not clearly visible or visible as a cold spot, a ROI technique was also used. A tumor-to-nontumor ratio (T/N ratio) was calculated from the PSR in tumor tissue and the PSR in contralateral normal tissue. In patients with rectal cancer, a nontumor PSR was calculated from the gluteal muscle because there were no data on normal rectal tissue in these patients. In all patients, SUVs were calculated from the last frame, using the following equation:

$$SUV = \frac{\text{tissue concentration (MBq/g)}}{\text{injected dose (MBq)/patient weight (g)}}.$$

Statistical analysis included the Wilcoxon test to compare the PSR in tumor tissue to that in the corresponding contralateral normal tissue, while the Mann-Whitney U-test was used to compare the difference in PSR, T/N ratio and SUV between malignant and benign tumors. A p value of < 0.05 was considered to be significant.

RESULTS

In 16 of 22 patients, a malignant tumor was proven by biopsy, while in the remaining six patients, a benign lesion was diagnosed histologically. Results of the PET studies are shown in Table 1.

Fifteen of the 16 malignancies (94%) were correctly identified as a hot spot. The one malignancy missed was a chondrosarcoma of the sacrum which had a very low malignancy grade. However, ROIs drawn at the tumor site, as indicated by CT, revealed a slightly higher PSR than in the contralateral normal tissue (T/N ratio 1.16). In a patient with ductal breast carcinoma, axillary hot spots were discovered in addition to the primary tumor, as the axillary region was also partly in the field of view (Fig. 1). These nonpalpable and previously unknown lesions were histologically confirmed to be metastases.

In the six patients with benign lesions, four (67%) were identified as cold spots. A benign schwannoma and an intramuscular hemangioma of the forearm were visualized as hot spots, whereas the other lesions had a PSR lower than the surrounding tissue. An example of a PET scan from a patient with a lipoma is shown in Figure 2. Necrosis within a malignant tumor was also visualized as a cold spot (Fig. 3).

Median PSR in normal tissue was 0.34 and ranged from 0.07 in breast tissue to 0.74 in normal gut tissue. PSR in tumor tissue was higher than in the corresponding contralateral normal tissue ($p = 0.0002$; one-tailed Wilcoxon). With a threshold PSR of 0.74 nmole/ml/min (the highest value obtained from normal tissue), the sensitivity and specificity of PET with TYR were 81% and 100%, respectively. The predictive value of a PSR $>$ 0.74 for having a malignant tumor was 100%, while the predictive value of a PSR of ≤ 0.74 for having a benign tumor was 67%. With a threshold PSR of 0.32 nmole/ml/min (the lowest value obtained from malignant tissue), the sensitivity and specificity were 100% and 83%, respectively. The predictive values for malignant and benign tumors were 94% and 100%, respectively (Fig. 4). The T/N ratio ranged from 1.16 to 8.77 in malignant tumors and from 0.40 to 1.78 in benign tumors. This difference was significant ($p = 0.00035$; one-tailed Mann-Whitney U-test). The SUV ranged from 0.97 to 6.94 in malignant tumors and from 0.09 to 1.17 in benign tumors. There was a moderate correlation between the PSR and the SUV of the tumors (correlation coefficient 0.76; Fig. 5). The PSR and SUV in malignant tumors were significantly higher than in the benign tumors ($p = 0.00025$; one-tailed Mann-

TABLE 1
Histology, Tumor Size and PET Visualization of all Tumors, PSR in Tumor Tissue and Contralateral Normal Tissue, T/N ratio and SUV

Patient no.	Histology	Tumor size (cm)	Visualization	PSR tumor (nmole/ml/min)	PSR contralat (nmole/ml/min)	T/N ratio	SUV
1	Synovial sarcoma	4.5	Hot spot	1.60	0.29	5.32	5.00
2	Mesenchymal chondrosarcoma	12.5	Hot spot	1.49	0.66	2.26	2.60
3	Unspecified sarcoma	16.0	Hot spot	1.54	0.49	3.14	4.05
4	Chondrosarcoma of bone	5.0	—	0.67	0.58	1.16	1.56
5	Malignant fibrous histiocytoma of bone	3.6	Hot spot	1.76	0.37	4.76	4.34
6	Melanoma	4.1	Hot spot	0.96	0.38	2.53	2.83
7	Melanoma	3.5	Hot spot	1.54	0.44	3.50	2.47
8	Melanoma	1.7	Hot spot	1.18	0.43	2.74	2.83
9	Breast cancer (lobular)	4.0	Hot spot	0.32	0.07	4.57	0.97
10	Breast cancer (ductal)	3.5	Hot spot	0.78	0.35	2.23	1.59
11	Breast cancer (ductal)	4.0	Hot spot	1.14	0.13	8.77	4.13
12	Rectal carcinoma	2.0	Hot spot	0.91	0.19	4.79	3.22
13	Rectal carcinoma	2.5	Hot spot	1.40	0.28	3.57	2.33
14	Rectal carcinoma	3.3	Hot spot	2.25	0.33	6.82	4.71
15	Metastasis from a non-seminoma testis	2.0	Hot spot	1.81	0.74	2.45	2.88
16	Squamous-cell carcinoma of the foot	2.0	Hot spot	1.19	0.14	8.50	6.94
17	Lipoma (benign)	24.0	Cold spot	0.18	0.34	0.53	0.82
18	Lipoma (benign)	2.0	Cold spot	0.08	0.20	0.40	0.36
19	Lipoma (benign)	14.0	Cold spot	0.13	0.30	0.42	0.09
20	Elastofibroma (benign)	8.0	Cold spot	0.14	0.23	0.65	0.66
21	Hemangioma (benign)	8.0	Hot area	0.16	0.09	1.78	0.59
22	Schwannoma (benign)	3.4	Hot spot	0.72	0.41	1.76	1.17

Contralat = contralateral normal tissue.

Whitney U-test). PSR, T/N ratio and SUV were not positively correlated with tumor size, which indicated that partial volume effects did not play any significant role in the quantification process.

DISCUSSION

These results show high uptake of TYR in various types of malignancy and low uptake in benign lesions. A comparative study on protein incorporation of different amino acids in tumor-bearing mice has proven the superiority of carboxyl-labeled tracers for measuring PSR (*24,25*). As such, TYR appears to be a good tracer. One malignant tumor was not visualized (i.e., a very low-grade malignant chondrosarcoma). Generally speaking, the detection of tumors depends on the difference between the intensity of the signal from the tumor and that from the background. Consequently, a false-negative result may be caused by a low tumor signal or by a high background signal. The latter depends on the localization of the tumor. Therefore, TYR will probably not be suitable for detecting liver, pancreas or salivary gland tumors because of the high PSR in these background tissues, although it is expected

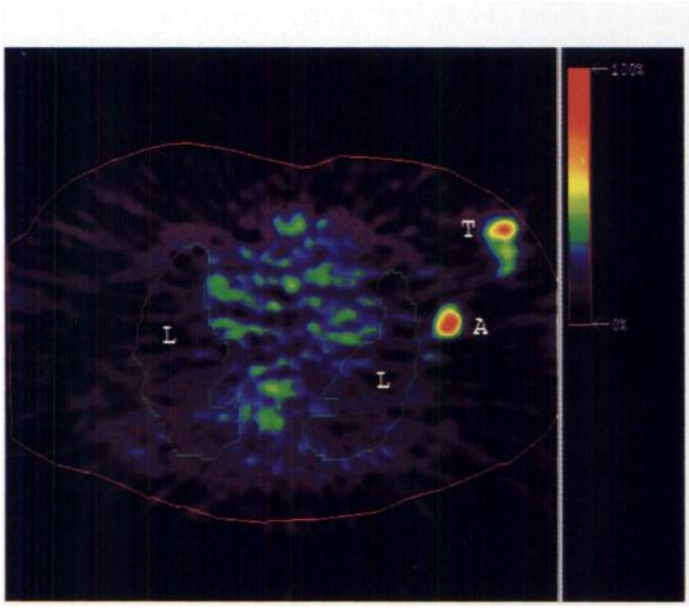

FIGURE 1. Transaxial PET slice of the thorax of Patient 11 with a 4-cm diameter ductal carcinoma (T) of the left breast that has a clearly visible metastasis in the axilla (A).

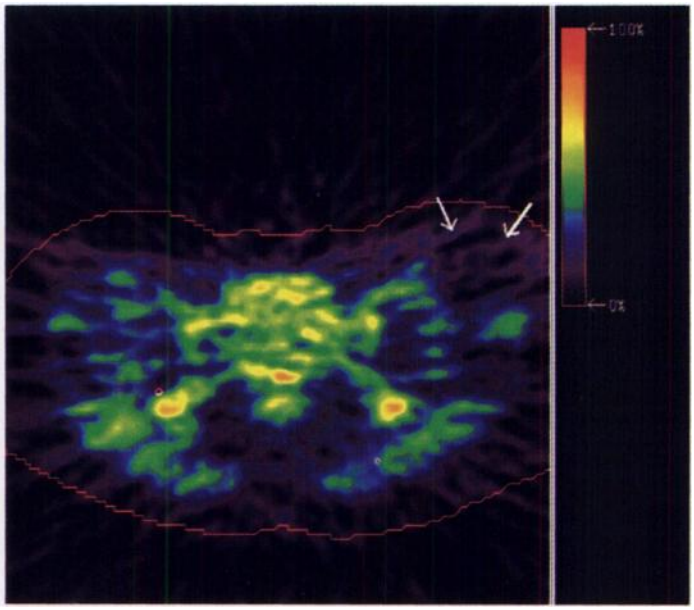

FIGURE 2. Transaxial PET slice of the pelvic region of Patient 19 with a 14-cm diameter lipoma in the right inguinal region (arrows). The lesion is visualized as a cold spot.

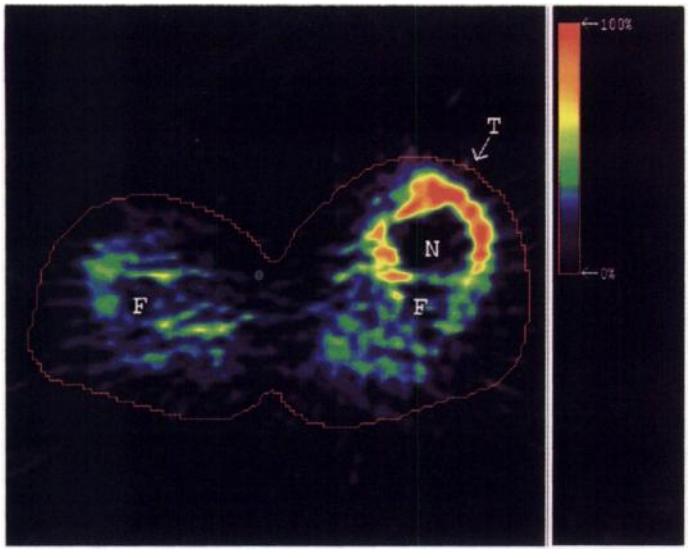

FIGURE 3. Transaxial PET slice of the upper legs of Patient 3 with a 16-cm diameter highly malignant sarcoma (T) in the right leg that has a central necrosis (N) (F=femur).

that TYR has advantages in the bladder region because it is not excreted with urine. In our false-negative case, the low PSR can probably be attributed to the known low metabolic activity of chondrosarcomas. However, as there was only one such patient in our series, further studies are needed to elucidate TYR uptake in chondrosarcomas.

As expected, benign lesions demonstrated a low PSR, especially lipomas which visualized as cold spots. However, two benign lesions were visualized as hot spots. The intramuscular hemangioma of the lower forearm in Patient 21 showed a higher TYR uptake than the background, but both the PSR and the SUV were very low. Therefore, this lesion was not suspected to be malignant. It has been suggested that TYR uptake in a tumor is related to blood flow, but the same authors show high uptake of TYR in poorly vascularized tumor regions (*26*). Furthermore, studies of transport in the brain showed that the fractional extraction of amino acids is low and their clearance is diffusion-limited and flow-independent at normal rates of blood flow (*27,28*).

The benign schwannoma in Patient 22 was visualized as a hot spot. It is known that tumors of neuroectodermal origin have a higher PSR than background tissue when they are located in the brain (*22*). Most of these brain tumors are only considered to be malignant because there is not enough room for them within the skull and not because of other malignant factors, such as the potential to metastasize. Normal brain tissue has an average PSR of approximately 0.50 nmole/ml/min, which is comparable with the background PSR in a leg, where this schwannoma was located. Therefore, a high PSR may be a common feature of neuroectodermal tumors both inside and outside the brain.

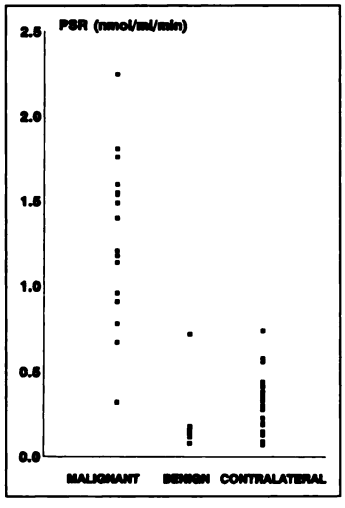

FIGURE 4. PSR in malignant tumors, benign lesions and normal tissues.

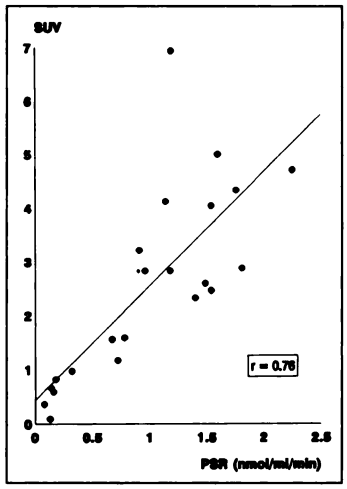

FIGURE 5. PSR plotted against SUV.

For simple tumor detection, quantification of the PSR (and therefore arterial cannulation) is not necessary. Calculating an SUV or a tumor-to-background ratio will be sufficient. However, for tumor therapy monitoring, the possibility of calculating a PSR may be of great value. For this reason, TYR has advantages over other amino acid tracers, such as methyl-labeled methionine. For instance, due to chemotherapy or radiotherapy, the normal background tissues are also likely to undergo a change in metabolic rate. To monitor the effects of treatment, a more objective quantification measure might be needed, such as PSR. This measure allows the comparison of uptake kinetics of different tracers, whereas SUVs cannot be compared between tracers because of differences in distribution over the body.

CONCLUSION

This early clinical study indicates that PET with TYR can visualize various types of tumors. The PSR could be quantified and was higher in malignant tumors than in normal tissue and the investigated benign lesions, although some overlap was present. Correlation of proliferation rate and malignancy grade with the PSR of tumors, as well as the differentiation of malignant tumors from inflammatory tissue are currently under investigation.

ACKNOWLEDGMENTS

Financial support provided by the Dutch Cancer Society (Koningin Wilhelmina Fonds) grant RUG 94-786. Part of this investigation was presented at the 48th Annual Cancer Symposium of the Society of Surgical Oncology, Boston, MA, March 23–26, 1995.

REFERENCES

1. Sasaki Y. Monitoring tumor radiotherapy. *J Nucl Med* 1991;32:2124–2125.
2. Royal HD. Clinical applications of positron emission tomography in cancer: the good, the bad and the ugly. *J Nucl Med* 1992;33:330–332.
3. Braams JW, Pruim J, Freling NJM, et al. Detection of lymph node metastases of squamous cell cancer in the head and neck with PET-FDG and MRI. *J Nucl Med* 1995;36:211–216.
4. Macfarlane DJ, Cotton L, Ackermann RJ, et al. Triple-head SPECT with 2-[fluorine-18]fluoro-2-deoxy-D-glucose (FDG): initial evaluation in oncology and comparison with FDG PET. *Radiology* 1995;194:425–429.
5. Hawkins RA, Phelps ME. PET in clinical oncology. *Cancer Metast Rev* 1988;7:119–142.
6. Kubota R, Yamada S, Kubota K, Ishiwata K, Tamahashi N, Ido T. Intratumoral distribution of fluorine-18-fluorodeoxyglucose in vivo: high accumulation in macro-

phages and granulation tissues studied by microautoradiography. *J Nucl Med* 1992; 33:1972–1980.
7. Lewis P, Salama A. Uptake of fluorine-18-fluorodeoxyglucose in sarcoidosis. *J Nucl Med* 1995;35:1647–1649.
8. Ishiwata K, Vaalburg W, Elsinga PH, Paans AMJ, Woldring MG. Metabolic studies with L-[1-^{14}C]tyrosine for the investigation of a kinetic model to measure protein synthesis rates with PET. *J Nucl Med* 1988;27:524–529.
9. Kubota K, Matsuzawa T, Fujiwara T, et al. Differential diagnosis of AH109A tumor and inflammation by radioscintigraphy with L-[methyl-^{11}C]methionine. *Jpn J Cancer Res* 1989;80:778–782.
10. Sato T, Fujiwara T, Abe Y, et al. Double-tracer whole-body autoradiography using a short-lived positron emitter and a long-lived beta emitter [Abstract]. *Radioisotopes* 1989;38:7–12.
11. Schober O, Meyer G-J, Duden C, et al. Uptake of amino acids in brain tumors using positron emission tomography as an indicator for assessing metabolic activity and malignancy. *Fortschr Röntgenstr* 1987;147:503–509.
12. Derlon J-M, Bourdet C, Bustany P, et al. Carbon-11-L-methionine uptake in gliomas. *Neurosurgery* 1989;25:720–728.
13. Lilja A, Lundqvist H, Olsson Y, Spännare B, Gullberg P, Långström B. Positron emission tomography and computed tomography in differential diagnosis between recurrent or residual glioma and treatment-induced brain lesions. *Acta Radiol* 1989; 30:121–128.
14. Daemen BJG, Elsinga PH, Ishiwata K, Paans AMJ, Vaalburg W. A comparative PET study using different ^{11}C-labeled amino acids in Walker 256 carcinosarcoma-bearing rats. *J Nucl Med Biol* 1991;18:197–204.
15. Ishiwata K, Vaalburg W, Elsinga PH, Paans AMJ, Woldring MG. Comparison of L-[1-^{11}C]methionine and L-methyl-[^{11}C]methionine for measuring in vivo protein synthesis rates with PET. *J Nucl Med* 1988;29:1419–1427.
16. Storch KJ, Wagner DA, Burke JF, Young VR. Quantitative study in vivo of methionine cycle in humans using [methyl-$^{2}H_3$]- and [1-^{13}C]methionine. *Am J Physiol* 1988;255:E322–E331.
17. Bolster JM, Vaalburg W, Paans AM, et al. Carbon-11-labeled tyrosine to study tumor metabolism by positron emission tomography (PET). *Eur J Nucl Med* 1986;12:321–324.
18. Keen RE, Barrio JR, Huang S-C, Hawkins RA, Phelps ME. In vivo cerebral protein synthesis rates with leucyl-transfer RNA used as a precursor pool: determination of biochemical to structure tracer kinetic models for positron emission tomography. *J Cereb Blood Flow Metab* 1989;9:429–445.
19. Phelps ME, Barrio JR, Huang S-C, Keen RA, Chugani H, Mazziotta JC. Criteria for the tracer kinetic measurement of cerebral protein synthesis in humans with positron emission tomography. *Ann Neurol* 1984;15(suppl):S192–S202.
20. Paans AMJ, Elsinga PH, Vaalburg W. Carbon-11-labeled tyrosine as a probe for modelling the protein synthesis rate. In: Mazoyer BM, Heiss WD, Comar D, eds. *PET studies on amino acid metabolism and protein synthesis.* Dordrecht: Kluwer; 1993: 161–174.
21. Willemsen ATM, Waarde A, van, Paans AMJ, et al. In vivo protein synthesis rate determination with L-[1-^{11}C]-tyrosine and positron emission tomography: methods, metabolism, modeling and results in patients with primary or recurrent brain tumors. *J Nucl Med* 1995;36:411–419.
22. Pruim J, Willemsen ATM, Molenaar WM, et al. L-[1-^{11}C]-tyrosine PET for visualization of brain tumors and quantitation of the protein synthesis rate. *Radiology* 1995;197:221–226.
23. Thorell J-O, Stone-Elander S, Elander N. Use of a microwave cavity to reduce reaction times in radiolabeling with [^{11}C]cyanide. *J Lab Compd Radiopharm* 1992;31:207–217.
24. Ishiwata K, Kubota K, Murakami M, Kubota R, Senda M. A comparative study on protein incorporation of L-[methyl-^{3}H]methionine, L-[1-^{14}C]leucine and L-2-[^{18}F]fluorotyrosine in tumor bearing mice. *Nucl Med Biol* 1993;20:895–899.
25. Ishiwata K, Kubota K, Murakami M, et al. Re-evaluation of amino acid PET studies: can the protein synthesis rates in brain and tumor tissues be measured in vivo? *J Nucl Med* 1993;34:1936–1943.
26. Carnochan P, Deehan B, Trivedi M, Tombs A, Sandle J, Ott R. Uptake of radiolabeled tyrosine and iodo-methyl tyrosine in experimental rat tumors; influence of blood flow and tumor growth rate. *J Nucl Biol Med* 1994;38(suppl 1):92–95.
27. Bradbury MWB, Patlak CS, Oldendorf WH. Analysis of brain uptake and loss of radiotracers after intracarotid injection. *Am J Physiol* 1975;229:1110–1115.
28. Oldendorf WH. Brain uptake of radiolabeled amino acids, amines and hexoses after arterial injection. *Am J Physiol* 1991;221:1629–1639.

Incremental Prognostic Value of Thallium Reinjection after Stress-Redistribution Imaging in Patients with Previous Myocardial Infarction and Left Ventricular Dysfunction

Mario Petretta, Alberto Cuocolo, Domenico Bonaduce, Emanuele Nicolai, Stefania Cardei, Sabino Berardino, Angiolino Ianniciello, Claudio Apicella, Valter Bianchi and Marco Salvatore

Institute of Internal Medicine, Cardiology and Heart Surgery; and Department of Nuclear Medicine and Nuclear Medicine Center of the National Research Council, Institute of Radiological Sciences, University of Naples, Naples, Italy

This study evaluated the incremental prognostic value of ^{201}Tl reinjection imaging over clinical, exercise and thallium stress-redistribution data in patients with previous myocardial infarction and left ventricular dysfunction. **Methods:** Thallium-201 reinjection after stress-redistribution SPECT was performed in 104 consecutive patients with a first Q-wave myocardial infarction (>8 wk) and left ventricular ejection fraction ≤40%. Follow-up data (mean 22 mo) were available for 98 patients; 16 patients underwent early revascularization procedures within 3 mo after exercise testing and were not considered for the analysis. **Results:** During follow-up there were 13 hard events (cardiac death and myocardial infarction) and 11 soft events (coronary revascularization procedures >3 mo after thallium imaging). With multivariate Cox regression analysis, the sum of defects at stress-redistribution imaging that were reversible or moderate irreversible after reinjection was a powerful predictor of subsequent events. The addition of thallium reinjection imaging data significantly improved the prognostic power of clinical, exercise and stress-redistribution data for the occurrence of hard events ($p < 0.01$). **Conclusion:** In patients with previous myocardial infarction and left ventricular dysfunction, thallium reinjection imaging provides incremental prognostic information over those obtained from conventional stress-redistribution imaging.

Key Words: myocardial infarction; left ventricular dysfunction; viable myocardium; thallium reinjection imaging

J Nucl Med 1997; 38:195–200

Stress-redistribution ^{201}Tl imaging is widely used to identify coronary artery disease in patients with chest pain (*1,2*). Furthermore, it has been demonstrated that the presence and the extent of transient defects have important prognostic value in coronary artery disease patients (*3–8*).

Thallium-201 reinjection after stress-redistribution enhances the identification of hypoperfused but viable myocardium (*9,10*), and its results are useful for management decisions in patients after myocardial infarction (*10,11*). Stress-redistribution reinjection thallium protocols, providing information concerning both jeopardized and viable myocardium, seem attractive for evaluating prognosis in patients with nonrecent myocardial infarction and left ventricular dysfunction (*11*). However, there are no data as yet available on the prognostic value of thallium reinjection after stress-redistribution in patients with chronic ischemic left ventricular dysfunction. This

Received Dec. 12, 1995; revision accepted June 15, 1996.

For correspondence or reprints contact: Domenico Bonaduce, MD, Via Aniello Falcone, 394, 80127 Napoli, Italy.